Pacejka Tire Model

Vehicle Dynamics, Planning and Control of Robotic Cars

Mattia Piccinini,
Gastone Pietro Papini Rosati

EIT Digital Master School
University of Trento

October 2021

Tire model

Accurate modeling of vehicle dynamics hugely depends on the level of knowledge of tire behavior. As a matter of fact, almost all reference books in the field of vehicle dynamics, like Guiggiani [2014], Jazar [2008] and Abe [2009], dedicate the first chapter to tire and wheel models. This is basically because tires are the only means from which a vehicle can get longitudinal force to accelerate and lateral force to steer. A deep understanding of tire behavior is particularly important when the vehicle is required to reach the limits of handling, which are mainly related to tire force saturation.
Several approaches are proposed in the literature to model tire performance. Each of these methods has some specific parameters that must be tuned basing on a tire testing campaign and/or experimental telemetry data. In this project the attention is focused on tire models specifically developed to be integrated within simulation environments. As a result, approaches based for instance on tire finite-element analysis will not be investigated since their applicability would be, in this context, extremely limited.
Tire models may be, in general, subdivided in two main categories: physical models and semi-empirical ones. The Brush model (see Pacejka [2012]) is one of the main examples of physical models, since it gives a physical interpretation for the mechanisms involved in longitudinal and lateral slip generation. On the contrary, semi-empirical models are only partially based on physical principles, since they contain particular structures deriving mainly from a fitting of experimental test data. Within this second category, many solutions may be found, depending on the desired accuracy and the affordable level of complexity. For example, Dugoff and Burckhardt models (refer to Dugoff et al. [1969] and Elmas et al. [2015], respectively) are relatively simple models and they may be able to predict tire behavior with a quite acceptable accuracy, which can be useful when designing driver assistance systems like ABS or ESP. However, probably the semi-empirical tire model with the greatest potential is the one introduced by Pacejka and based on the so-called Magic Formula, described in detail in Pacejka [2012]. Several formulations of the Magic Formula have been developed since 1958, and the most suitable version should be chosen for each application, mainly depending on the available experimental data. For this project, the *Pacejka 1996* model is used, basing on Pacejka [1996].
Pacejka model allows a high-fidelity representation of *steady-state* tire behavior.
First of all, a local tire reference frame RF_t needs to be defined. Assuming initially that the tire is a rigid component, the origin of RF_t is located in the tire-road geometrical contact point. The horizontal x_t axis points forward in the rolling direction, while the z_t axis is vertical and directed upwards. Figure 1 shows the local tire frame as well as the main forces and moments that are now going to be explained.

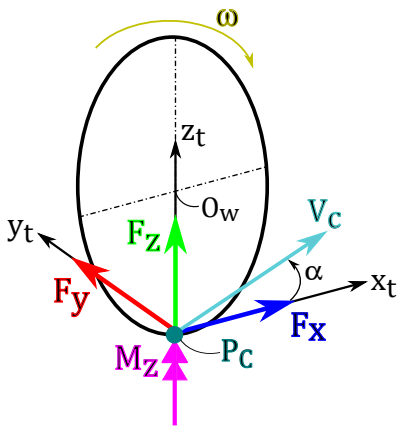

Figure 1: Tire reference frame and tire forces/moments

Considering now that the tire is a deformable body, then a contact patch exists between tire and ground. It can be shown that slippage needs to occur within the contact area in order for the tire to produce the basic forces that allow a vehicle to accelerate, brake and steer. The rubber polymeric material composing the tire has viscoelastic properties, enabling energy dissipation and hysteresis mechanisms that are involved in slip build up processes. Tire slip is mainly explained by the two physical phenomena of indentation and adhesion. The former involves the partial penetration of road roughness asperities into the tire tread, while the latter is the result of Van der Waals interactions at the rubber-ground interface. As a particle of rubber tread enters the road contact region, compression and shear deformation initially occur, followed by a slippage phase that can lead to the development of tire longitudinal and/or lateral macroscopic forces/moments.
Being $\vec{\omega}$ the tire angular speed, O_w the wheel center and P_c the tire-road (theoretical) contact point (as depicted in Figure 1), the rolling velocity $\vec{v}_R$ is defined as:

$$\vec{v}_R = \vec{\omega} \wedge \overrightarrow{O_w P_c} \tag{1}$$

The absolute value $|\vec{v}_R|$ is equal to ωR_e, where R_e is the effective rolling radius (which can be computed in free rolling conditions by dividing the longitudinal component of the total velocity vector of wheel center by ω).
Referring to Figure 2, the sliding velocity $\vec{v}_S$ is the difference of the total contact point velocity $\vec{v}_C$ and $\vec{v}_R$:

$$\vec{v}_S = \vec{v}_C - \vec{v}_R \tag{2}$$

During acceleration, it is $|\vec{v}_R| > |\vec{v}_{Cx}|$, and so $v_{Sx} < 0$. Conversely, in braking

phases it is $|\vec{v}_R| < |\vec{v}_{Cx}|$, meaning that $v_{Sx} > 0$. Pure rolling conditions are achieved when $\vec{v}_C = \vec{v}_R$, so that $\vec{v}_S = 0$.

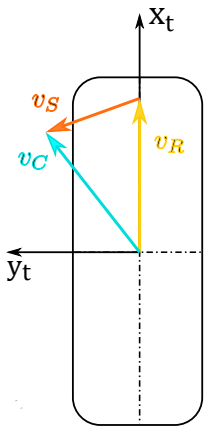

Figure 2: Tire top view: sliding velocity as the difference of contact point velocity and rolling velocity

Theoretical slip is given by:

$$\vec{\sigma} = \begin{pmatrix} \sigma_x \\ \sigma_y \end{pmatrix} = -\frac{\vec{v}_S}{|\vec{v}_R|} = \begin{pmatrix} -v_{Sx}/|\vec{v}_R| \\ -v_{Sy}/|\vec{v}_R| \end{pmatrix} \tag{3}$$

Pacejka model actually uses practical slips κ and α, defined as:

$$\vec{\sigma}_{\text{pract}} = \begin{pmatrix} \kappa \\ \tan(\alpha) \end{pmatrix} = -\frac{\vec{v}_S}{|\vec{v}_{Cx}|} = \begin{pmatrix} -v_{Sx}/|\vec{v}_{Cx}| \\ -v_{Sy}/|\vec{v}_{Cx}| \end{pmatrix} \tag{4}$$

The slip vector has therefore two components, with κ called longitudinal slip and α being the side slip angle. κ and α are usually expressed as:

$$\kappa = \frac{\omega R_e - v_{Cx}}{v_{Cx}} \tag{5}$$

$$\alpha = -\arctan\left(\frac{v_{Cy}}{v_{Cx}}\right) \tag{6}$$

In (5) and (6), $\{v_{Cx}, v_{Cy}\}$ are expressed with respect to the local tire reference frames.

If the wheel is accelerating then κ is positive, and a positive longitudinal tire force F_x is consequently generated. On the other hand, during braking it is $\kappa < 0$ and a negative F_x is produced. The case with $\kappa = -1$ corresponds to wheel lock.
It will be shown that longitudinal tire force F_x, lateral tire force F_y and the self-aligning torque M_z (see Figure 1) are all functions of both κ and α. Moreover, other important factors influencing tire forces and moments are the vertical wheel load F_z and the camber γ. Following Pacejka [2012], camber is the inclination angle of the wheel plane about the x_t axis. γ is positive when the wheel appears to be tilted to the right when looking from behind. A tire with $\gamma > 0$ generates a negative lateral force F_y, as depicted in Figure 3.

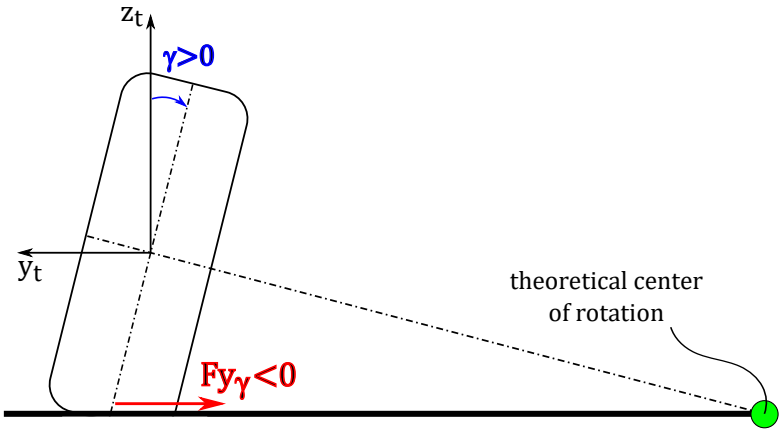

Figure 3: Positive camber γ generates a negative tire lateral force F_y

As it was explained in the introductory part of this Section, experimental test data are always the base point from which to start, for the identification of tire behavior. An effective way for collecting tire data is to perform laboratory tests in a controlled environment, with the so-called tire test rig. This is what was done by the Formula SAE Tire Test Consortium (TTC) at the Calspan Tire Test Facility (TIRF), in Buffalo (USA). This association yearly schedules specific tests to be carried out on Formula SAE tires. Test results are then sold to teams, and all tire data presented in this work were bought from TTC.
In laboratory tests, the road surface is simulated with a flat belt, while tire forces and moments are measured with a special hub. Longitudinal and later slips, vertical load, camber and speed can be varied within each test.
The data that are henceforth used refer to the *Hoosier* 18x6 − 10 LCO tires, whose performance is believed to be close to the one provided by the actual tires mounted on the vehicle *Chimera Evoluzione*. TTC data are subdivided in three main categories: pure longitudinal acceleration/brake tests, pure lateral tests and combined longitudinal/lateral tests.

Figure 4 shows some of the raw data for pure longitudinal tests. Notice that, as the longitudinal slip κ increases, the tire force F_x also increases until reaching a saturation value that depends on vertical F_z (expressed in pounds $[Ibs]$ in plot legends) and camber γ.

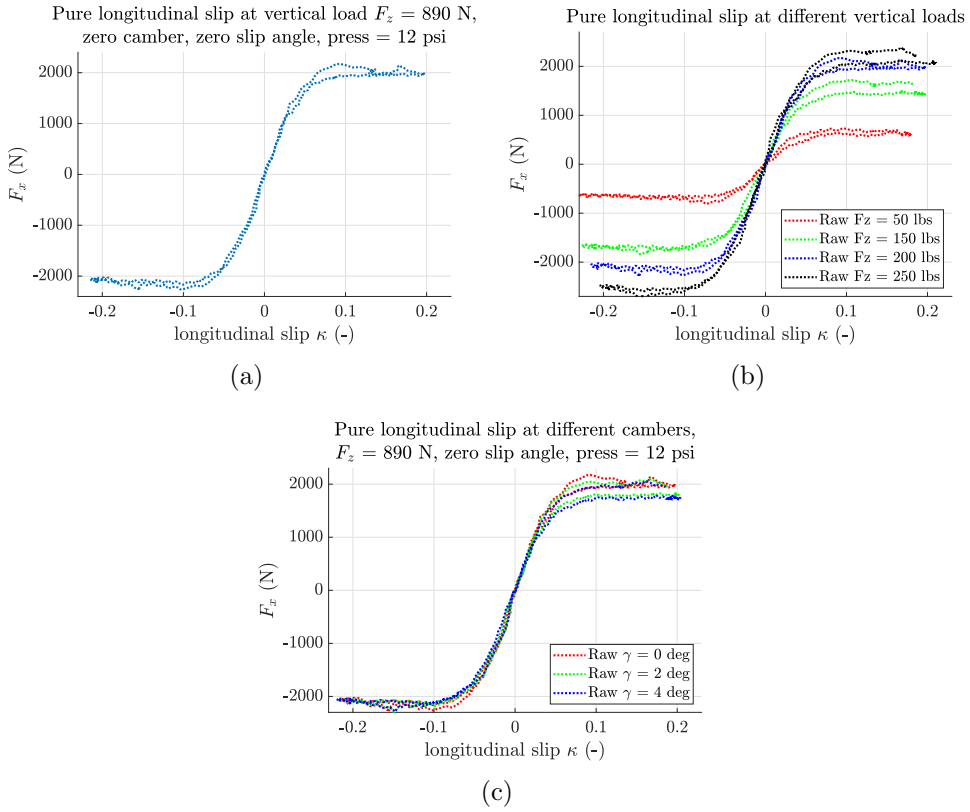

Figure 4: Raw experimental data from TTC, pure longitudinal slip tests

Figure 5 plots the raw data for pure lateral tests, showing the behavior of the lateral force F_y as a function of the side slip angle α. Notice that even for F_y a saturation limit exists, depending on F_z and γ.
Finally, Figure 6 depicts the behavior of the self-aligning torque M_z.
Judging from the graphs, it may be seen that, as the vertical wheel load F_z increases, tire forces and moments increase as well, but the dependency is non linear and a saturation exists even in this behavior. The main role of camber is instead that of introducing a vertical offset in the curves.

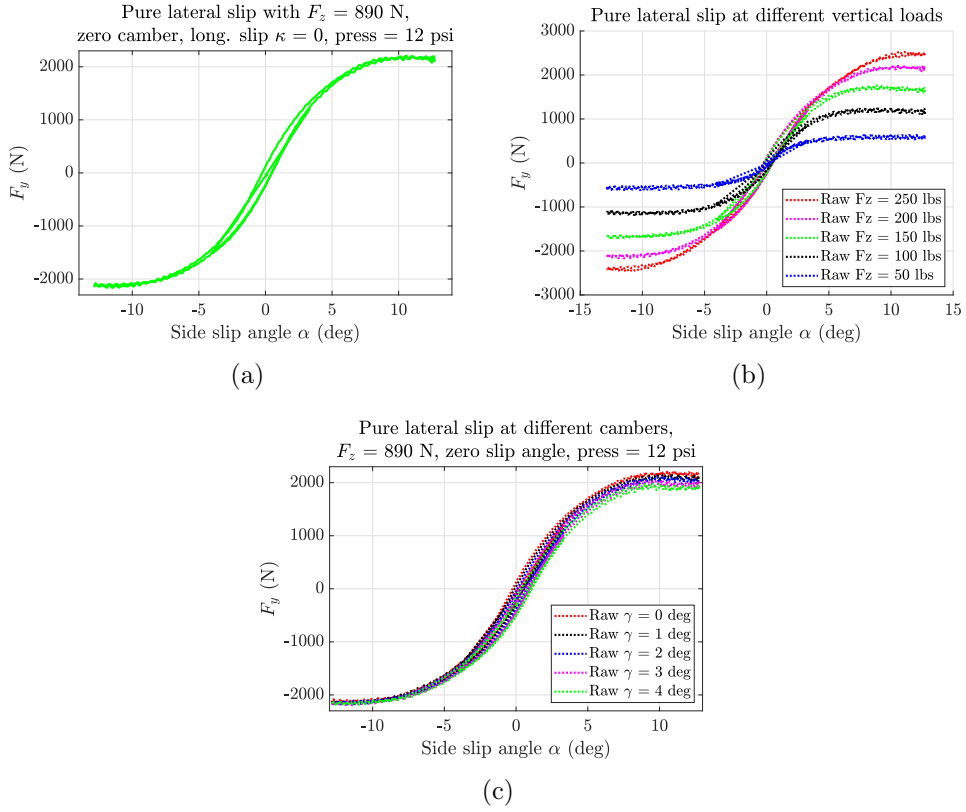

Figure 5: Raw experimental data from TTC, pure lateral slip tests, cornering force F_y results

Pacejka Magic Formula is an efficient tool to fit the curves shown above, so as to accurately predict tire performance in the various operating conditions.
Following Pacejka [2012], the approach makes use of the so-called *similarity method*, which is based on experimental evidence and suggests that pure (longitudinal or lateral) slip curves remain approximately similar in shape even when the tire operates in conditions that differ from the reference ones. The latter are defined in terms of nominal vertical wheel load F_{z0}, zero camber ($\gamma = 0$), with a given road surface (friction coefficient μ_0) and under the assumption of either free rolling ($\kappa = 0$) or zero side slip angle ($\alpha = 0$). Pacejka proved that, employing suitable normalizations and shifting of a tire force or moment curve under any working condition, the original reference curve for the same force/moment can be again obtained.

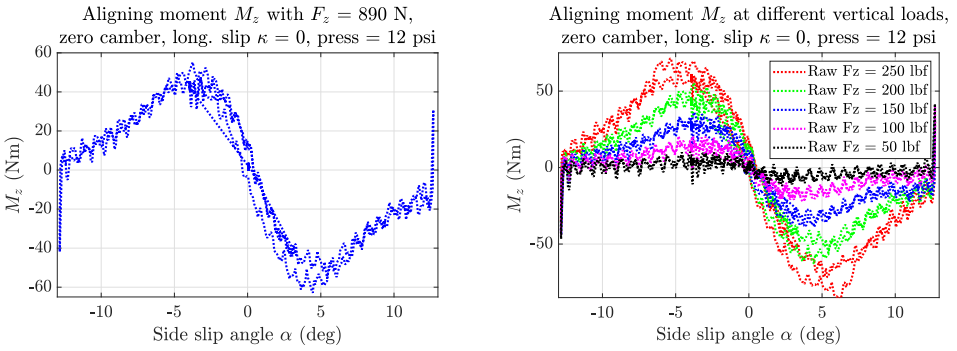

(a) (b)

Figure 6: Raw experimental data from TTC, pure lateral slip tests, self-aligning torque M_z results

The general form of the Pacejka Magic Formula, that holds for given values of vertical wheel load and camber angle, is the following:

$$y(x) = D \sin\Big(C \arctan\Big(Bx - E(Bx - \arctan(Bx))\Big)\Big), \tag{7}$$

with $Y(X) = y(x) + S_V$, $x = X + S_H$. The input variable is X, which can be either κ or $\tan(\alpha)$, while Y is the formula output, that may be the *steady-state* value of F_x, F_y or M_z. The parameter B is usually referred to as stiffness factor, C is the shape factor, D is the peak value, E is the curvature factor, while S_H and S_V are horizontal and vertical shifts, respectively. A graphical interpretation of these parameters is shown in Figure 7. Notice that the product BCD corresponds to the slope at the origin, for $x = y = 0$.

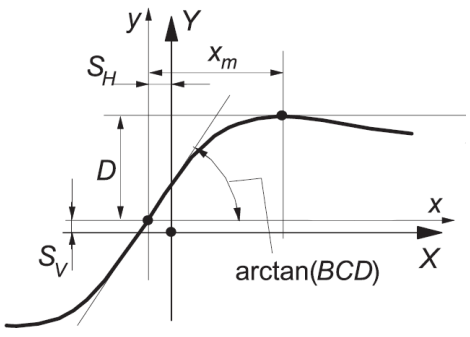

Figure 7: Graphical meaning of the Magic Formula parameters. Image taken from Pacejka [2012]

Returning to the similarity method, naming $F_y = F_{y0}(\alpha)$ the cornering force curve obtained under reference conditions ($F_z = F_{z0}$, $\gamma = 0$, $\kappa = 0$, friction coefficient μ_0), the effect of parameters variation may now be investigated. For example, if the vertical wheel load F_z varies, then both the peak value and the slope at the origin for F_y have to be modified accordingly. In order for this to be done, an initial scaling of a factor F_z/F_{z0} is performed so as to change the saturation limit of F_y. However, this scaling should not affect the slope at the origin, and for this reason the side slip α needs to be replaced with $\alpha F_{z0}/F_z$:

$$F_y = \frac{F_z}{F_{z0}} \cdot F_{y0}\left(\frac{F_{z0}}{F_z}\alpha\right) \tag{8}$$

Naming $C_{F\alpha 0} = \frac{\partial F_y}{\partial \alpha}|_{\alpha=0}$ the slope in $\alpha = 0$ (also called cornering stiffness) for the original reference curve, then it may be noticed that this quantity is not modified by the transformation operated in (8). In order to take into account the new value of cornering stiffness $C_{F\alpha}$ resulting from the change of F_z, the following manipulation is performed:

$$F_y = \frac{F_z}{F_{z0}} \cdot F_{y0}\left(\frac{C_{F\alpha}(F_z)}{C_{F\alpha 0}}\frac{F_{z0}}{F_z}\alpha\right) \tag{9}$$

In a similar fashion, the behavior of the self-aligning torque M_z as a function of F_z may be written as:

$$M_z = \frac{F_z}{F_{z0}}\frac{C_{M\alpha}(F_z)}{C_{M\alpha 0}}\frac{C_{F\alpha 0}}{C_{F\alpha}(F_z)} M_{z0}\left(\frac{C_{F\alpha}(F_z)}{C_{F\alpha 0}}\frac{F_{z0}}{F_z}\alpha\right), \tag{10}$$

with $M_{z0}(\alpha)$ being the self-aligning moment curve obtained in the nominal reference conditions, while $C_{M\alpha 0}$ and $C_{M\alpha}(F_z)$ are the torque stiffnesses (slopes at the origin $\alpha = 0$) for the reference and the vertical load variation cases, respectively.
The stiffnesses $C_{F\alpha}(F_z)$ and $C_{M\alpha}(F_z)$ depend on F_z and they tend to saturate for moderately high values of vertical load, as depicted in Figure 8.
Referring to (7), the expression of the lateral tire force F_{y0} at a certain vertical load F_{z0} is:

$$F_{y0} = D_{y0}\sin\Big(C_y \arctan\Big(B_{y0}\alpha - E_y(B_{y0}\alpha - \arctan(B_{y0}\alpha))\Big)\Big) \tag{11}$$

In (11), the peak factor D_{y0} is equal to $\mu_{y0}F_{z0}$.
Assuming now that the peak adherence μ_y is different from μ_{y0}, the expression of F_y is modified to take into account that the saturation limit is shifted vertically, but the cornering stiffness $C_{F\alpha}$ is not changed:

$$F_y = \frac{\mu_y}{\mu_{y0}} \frac{F_z}{F_{z0}} \cdot F_{y0} \left(\frac{C_{F\alpha}(F_z)}{C_{F\alpha 0}} \frac{\mu_{y0}}{\mu_y} \frac{F_{z0}}{F_z} \alpha \right) \tag{12}$$

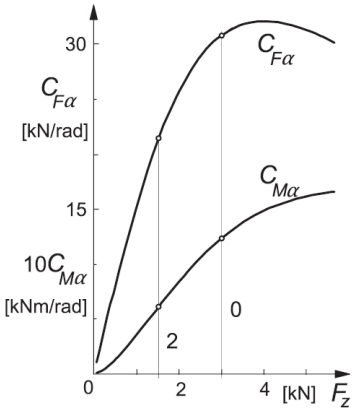

Figure 8: Behavior of the stiffnesses $C_{F\alpha}$ and $C_{M\alpha}$ as a function of F_z. Image taken from Pacejka [2012]

Finally, camber variations with respect to the reference configuration (that is for $\gamma = 0$) may be modeled by modifying the expression of the side slip angle α:

$$F_y = \frac{\mu_y}{\mu_{y0}} \frac{F_z}{F_{z0}} \cdot F_{y0} \left(\frac{C_{F\alpha}(F_z)}{C_{F\alpha 0}} \frac{\mu_{y0}}{\mu_y} \frac{F_{z0}}{F_z} \left(\alpha + \frac{C_{F\gamma}(F_z)}{C_{F\alpha}(F_z)} \gamma \right) \right) \tag{13}$$

Camber effect on self-aligning torque produces a horizontal and vertical shift. The vertical offset is expressed in terms of residual torque M_{zr}:

$$M_z = \frac{\mu_y}{\mu_{y0}} \frac{F_z}{F_{z0}} \frac{C_{M\alpha}(F_z)}{C_{M\alpha 0}} \frac{C_{F\alpha 0}}{C_{F\alpha}(F_z)} M_{z0} \left(\frac{C_{F\alpha}(F_z)}{C_{F\alpha 0}} \frac{\mu_y 0}{\mu_y} \frac{F_{z0}}{F_z} \left(\alpha + \frac{C_{F\gamma}(F_z)}{C_{F\alpha}(F_z)} \gamma \right) \right) + M_{zr} \tag{14}$$

Similar considerations hold for the influence of F_z and peak adherence μ_x on the longitudinal tire force F_x:

$$F_x = \frac{\mu_x}{\mu_{x0}} \frac{F_z}{F_{z0}} \cdot F_{x0} \left(\frac{C_{F\kappa}(F_z)}{C_{F\kappa 0}} \frac{\mu_{x0}}{\mu_x} \frac{F_{z0}}{F_z} \kappa \right) \tag{15}$$

Several methods may be adopted to study the combined slip case, i.e. the influence of longitudinal slip on the lateral force F_y and moment M_z, and the effect of side slip on F_x. One of the most efficient methods is to use the *cosine version* of the Magic Formula as a weighting function G for the pure slip forces and moments:

$$G = D\cos(C\arctan(Bx)), \tag{16}$$

with x being either κ or $\tan(\alpha)$ (possibly shifted). The weighting function G has a hill shape, with a peak value equal to D for $x = 0$, while C and B determine the height of the hill base and the hill steepness, respectively.
(17) reports the combined versions of the lateral and longitudinal tire forces:

$$\begin{cases} F_y = G_{yk}F_{y0} + S_{Vyk} \\ F_x = G_{xa}F_{x0} \end{cases} \tag{17}$$

Moreover, scaling factors λ_i are introduced in the Magic Formula so as to allow a potentially quick model adaptation to a changing friction coefficient, cornering stiffness or other parameters. These scaling factors will not be considered in this work (all λ_i are here set to one).
The normalized change in vertical load is defined as:

$$\mathrm{d}f_z = \frac{F_z}{F_{z0}} - 1, \tag{18}$$

with F_{z0} being the vertical load in reference conditions.
The full set of Pacejka 1996 equations is now summarized.
The formulas needed to compute the longitudinal force in the pure longitudinal (F_{x0}) and combined (F_x) cases are collected in (20). The coefficients that are to be fitted basing on experimental test data are:

$$\begin{aligned} \text{fitCoeffs\_pureLong} = \{&p_{Cx1}, p_{Dx1}, p_{Dx2}, p_{Dx3}, p_{Ex1}, p_{Ex2}, p_{Ex3}, p_{Ex4}, p_{Kx1}, p_{Kx2}, \dots \\ &p_{Kx3}, p_{Hx1}, p_{Hx2}, p_{Vx1}, p_{Vx2}\} \end{aligned} \tag{19}$$

The fitting can be performed using a least-squares algorithm. From a practical viewpoint, it is useful to split the fitting operations in three main steps, since the amount of coefficients to be tuned is quite high and many local minima might be found. In a first phase, only test data with $\mathrm{d}f_z = 0$ and camber $\gamma = 0$ may be used, so as to fit only the parameters $\{p_{Cx1}, p_{Dx1}, p_{Ex1}, p_{Ex4}, p_{Kx1}, p_{Hx1}, p_{Vx1}\}$.

Secondly, test data with different values of vertical loads ($\mathrm{d}f_z \neq 0$) but still $\gamma = 0$ can be considered, with the aim of fitting the only coefficients related to the $\mathrm{d}f_z$ term, namely $\{p_{Dx2}, p_{Ex2}, p_{Ex3}, p_{Kx2}, p_{Kx3}, p_{Hx2}, p_{Vx2}\}$. Thirdly, attention can be restricted to tests with nominal vertical load ($\mathrm{d}f_z = 0$) and non-zero camber γ, so as to fit the parameter p_{Dx3}.

$$
\begin{cases}
S_{Hx} = p_{Hx1} + p_{Hx2} \cdot \mathrm{d}f_z \\
\kappa_x = \kappa + S_{Hx} \\
C_x = p_{Cx1} \\
\mu_x = (p_{Dx1} + p_{Dx2} \cdot \mathrm{d}f_z)(1 - p_{Dx3}\gamma^2) \\
D_x = \mu_x F_z \\
K_{xk} = F_z(p_{Kx1} + p_{Kx2} \cdot \mathrm{d}f_z) \cdot e^{-(p_{Kx3} \cdot \mathrm{d}f_z)} \\
E_x = (p_{Ex1} + p_{Ex2} \cdot \mathrm{d}f_z + p_{Ex3} \cdot \mathrm{d}f_z^2)(1 - p_{Ex4}\mathrm{sign}(\kappa_x)) \\
B_x = K_{xk}/(C_x D_x) \\
S_{Vx} = F_z(p_{Vx1} + p_{Vx2} \cdot \mathrm{d}f_z) \\
S_{Hxa} = r_{Hx1} \\
B_{xa} = r_{Bx1} \cos(\arctan(\kappa \cdot r_{Bx2})) \\
C_{xa} = r_{Cx1} \\
D_{xa} = 1/\cos(C_{xa} \arctan(B_{xa} S_{Hxa})) \\
G_{xa} = D_{xa} \cos(C_{xa} \arctan(B_{xa}(\alpha + S_{Hxa}))) \\
F_{x0} = D_x \sin\Big(C_x \arctan\Big(B_x\kappa_x - E_x(B_x\kappa_x - \arctan(B_x\kappa_x))\Big)\Big) + S_{Vx} \\
F_x = G_{xa} F_{x0}
\end{cases}
\tag{20}
$$

As far as the combined longitudinal performance is concerned, referring to (20) the Pacejka parameters to be identified are summarized in (21), and they can be computed in a single fitting operation.

$$
\text{fitCoeffs\_combLong} = \{r_{Bx1}, r_{Bx2}, r_{Cx1}, r_{Hx1}\} \tag{21}
$$

The complete expression of the lateral tire force in pure (F_{y0}) and combined (F_y) cases is reported in (23). The fitting parameters are:

$$
\begin{aligned}
\text{fitCoeffs\_pureLateral\_Fy} = \{&p_{Cy1}, p_{Dy1}, p_{Dy2}, p_{Dy3}, p_{Ey1}, p_{Ey2}, p_{Ey3}, p_{Ey4}, p_{Hy1}, \dots \\
&p_{Hy2}, p_{Hy3}, p_{Ky1}, p_{Ky2}, p_{Ky3}, p_{Vy1}, p_{Vy2}, p_{Vy3}, p_{Vy4}\}
\end{aligned}
\tag{22}
$$

Even in this case it is convenient to subdivide the fitting in three steps. In a first phase only the test data with $F_z = F_{z0}$ (i.e. $\mathrm{d}f_z = 0$) and zero camber γ can be taken into account, so as to determine $\{p_{Cy1}, p_{Dy1}, p_{Ey1}, p_{Hy1}, p_{Ky1}, p_{Ky2}, p_{Vy1}\}$. It is then possible to use data with different values of $\mathrm{d}f_z$ but zero camber, so as to fit the coefficients $\{p_{Dy2}, p_{Ey2}, p_{Hy2}, p_{Vy2}\}$. In a third step, the data with $\gamma \neq 0$ can be employed with the target of computing $\{p_{Dy3}, p_{Ey3}, p_{Ey4}, p_{Hy3}, p_{Ky3}, p_{Vy3}, p_{Vy4}\}$.

$$
\begin{cases}
S_{Hy} = p_{Hy1} + p_{Hy2} \cdot \mathrm{d}f_z + p_{Hy3}\gamma \\
\alpha_y = \alpha + S_{Hy} \\
C_y = p_{Cy1} \\
\mu_y = (p_{Dy1} + p_{Dy2} \cdot \mathrm{d}f_z)(1 - p_{Dy3}\gamma^2) \\
D_y = \mu_y F_z \\
K_{ya} = F_{z0} \cdot p_{Ky1} \sin(2 \arctan(F_z/(F_{z0} p_{Ky2})))(1 - p_{Ky3}|\gamma|) \\
E_y = (p_{Ey1} + p_{Ey2} \cdot \mathrm{d}f_z)(1 - (p_{Ey3} - p_{Ey4}\gamma)\mathrm{sign}(\alpha_y)) \\
B_y = K_{ya}/(C_y D_y) \\
S_{Vy} = F_z\Big(p_{Vy1} + p_{Vy2}\mathrm{d}f_z + (p_{Vy3} + p_{Vy4}\mathrm{d}f_z)\gamma\Big) \\
D_{Vyk} = \mu_y F_z (r_{Vy1} + r_{Vy2}\mathrm{d}f_z + r_{Vy3}\gamma)\cos(\arctan(r_{Vy4}\alpha)) \\
S_{Vyk} = D_{Vyk} \sin(r_{Vy5} \arctan(r_{Vy6}\kappa)) \\
S_{Hyk} = r_{Hy1} \\
B_{yk} = r_{By1} \cos\Big(\arctan(r_{By2}(\alpha - r_{By3}))\Big) \\
C_{yk} = r_{Cy1} \\
D_{yk} = 1/\cos(C_{yk} \arctan(B_{yk} S_{Hyk})) \\
G_{yk} = D_{yk} \cos(C_{yk} \arctan(B_{yk}(\kappa + S_{Hyk}))) \\
F_{y0} = D_y \sin\Big(C_y \arctan\Big(B_y\alpha_y - E_y(B_y\alpha_y - \arctan(B_y\alpha_y))\Big)\Big) + S_{Vy} \\
F_y = G_{yk} F_{y0} + S_{Vyk}
\end{cases}
\tag{23}
$$

In the combined lateral slip case, notice the dependence of the weighting function G_{yk} upon $\mathrm{d}f_z$ and γ. This dependency may actually be neglected, in order to slightly simplify the model, by setting to zero r_{Vy2} and r_{Vy3}. The remaining coefficients are collected in (24), and they can now be fitted.

$$
\mathrm{fitCoeffs\_combLateral\_Fy} = \{r_{By1}, r_{By2}, r_{By3}, r_{Cy1}, r_{Hy1}, r_{Vy1}, r_{Vy4}, r_{Vy5}, r_{Vy6}\} \tag{24}
$$

The Pacejka formulas to compute the self-aligning torque M_{z0} are reported in (26). The combined slip case is not considered for M_z mainly due to the few available

combined test data. The fitting coefficients are:

$$\begin{aligned}\text{fitCoeffs\_pureLateral\_Mz} = \{&q_{Bz1}, q_{Bz2}, q_{Bz3}, q_{Bz4}, q_{Bz5}, q_{Bz9}, q_{Bz10}, q_{Cz1}, q_{Dz1}, \dots \\ &q_{Dz2}, q_{Dz3}, q_{Dz4}, q_{Dz6}, q_{Dz7}, q_{Dz8}, q_{Dz9}, q_{Ez1}, q_{Ez2}, \dots \\ &q_{Ez3}, q_{Ez4}, q_{Ez5}, q_{Hz1}, q_{Hz2}, q_{Hz3}, q_{Hz4}, R_o\}\end{aligned} \tag{25}$$

The fitting is again carried out in three phases. Experimental data obtained with $\mathrm{d}f_z = 0$ and $\gamma = 0$ allow to fit $\{q_{Bz1}, q_{Bz9}, q_{Bz10}, q_{Cz1}, q_{Dz1}, q_{Dz6}, q_{Ez1}, q_{Ez4}, q_{Hz1}\}$. Next, the data with $F_z \neq F_{z0}$ and $\gamma = 0$ enable the determination of $\{q_{Bz2}, q_{Bz3}, \dots$ $q_{Dz2}, q_{Dz7}, q_{Ez2}, q_{Ez3}, q_{Hz2}\}$. Finally, using tests with $\gamma \neq 0$ also the remaining parameters $\{q_{Bz4}, q_{Bz5}, q_{Dz3}, q_{Dz4}, q_{Ez5}, q_{Dz8}, q_{Dz9}, q_{Hz3}, q_{Hz4}\}$ can be identified.

$$\begin{cases} S_{Ht} = q_{Hz1} + q_{Hz2} \cdot \mathrm{d}f_z + (q_{Hz3} + q_{Hz4} \cdot \mathrm{d}f_z)\gamma \\ \alpha_t = \alpha + S_{Ht} \\ B_t = (q_{Bz1} + q_{Bz2} \cdot \mathrm{d}f_z + q_{Bz3} \cdot (\mathrm{d}f_z)^2)(1 + q_{Bz4}\gamma + q_{Bz5}|\gamma|) \\ C_t = q_{Cz1} \\ D_t = F_z(q_{Dz1} + q_{Dz2} \cdot \mathrm{d}f_z)(1 + q_{Dz3}\gamma + q_{Dz4}\gamma^2)(R_o/F_{z0}) \\ E_t = (q_{Ez1} + q_{Ez2} \cdot \mathrm{d}f_z + q_{Ez3} \cdot (\mathrm{d}f_z)^2)(1 + (q_{Ez4} + q_{Ez5}\gamma)\arctan(B_t C_t \alpha_t)) \\ S_{Hf} = S_{Hy} + S_{Vy}/K_{ya} \\ \alpha_r = \alpha + S_{Hf} \\ B_r = q_{Bz9} + q_{Bz10} B_y C_y \\ D_r = F_z\Big(q_{Dz6} + q_{Dz7} \cdot \mathrm{d}f_z + (q_{Dz8} + q_{Dz9} \cdot \mathrm{d}f_z)\gamma\Big) R_o \\ M_{zr} = D_r \cos(\arctan(B_r \alpha_r)) \cos(\alpha) \\ t = D_t \cos\Big(C_t \arctan\big(B_t\alpha_t - E_t(B_t\alpha_t - \arctan(B_t\alpha_t))\big)\Big) \cos(\alpha) \\ M_{z0} = -tF_y + M_{zr} \end{cases} \tag{26}$$

In the formulas (23) and (26) for the side force F_y and the aligning torque M_z, the vertical and horizontal offsets $\{S_{Vy}, S_{Hy}\}$, as well as the residual peak torque value D_r, may produce $F_y \neq 0$ and $M_z \neq 0$ even for $\alpha = 0$. This occurs to model the so-called *conicity* and *ply-steer* effects, which are related to asymmetries in the tire construction.
The main fitting results are shown in Figure 9, 10 and 11.

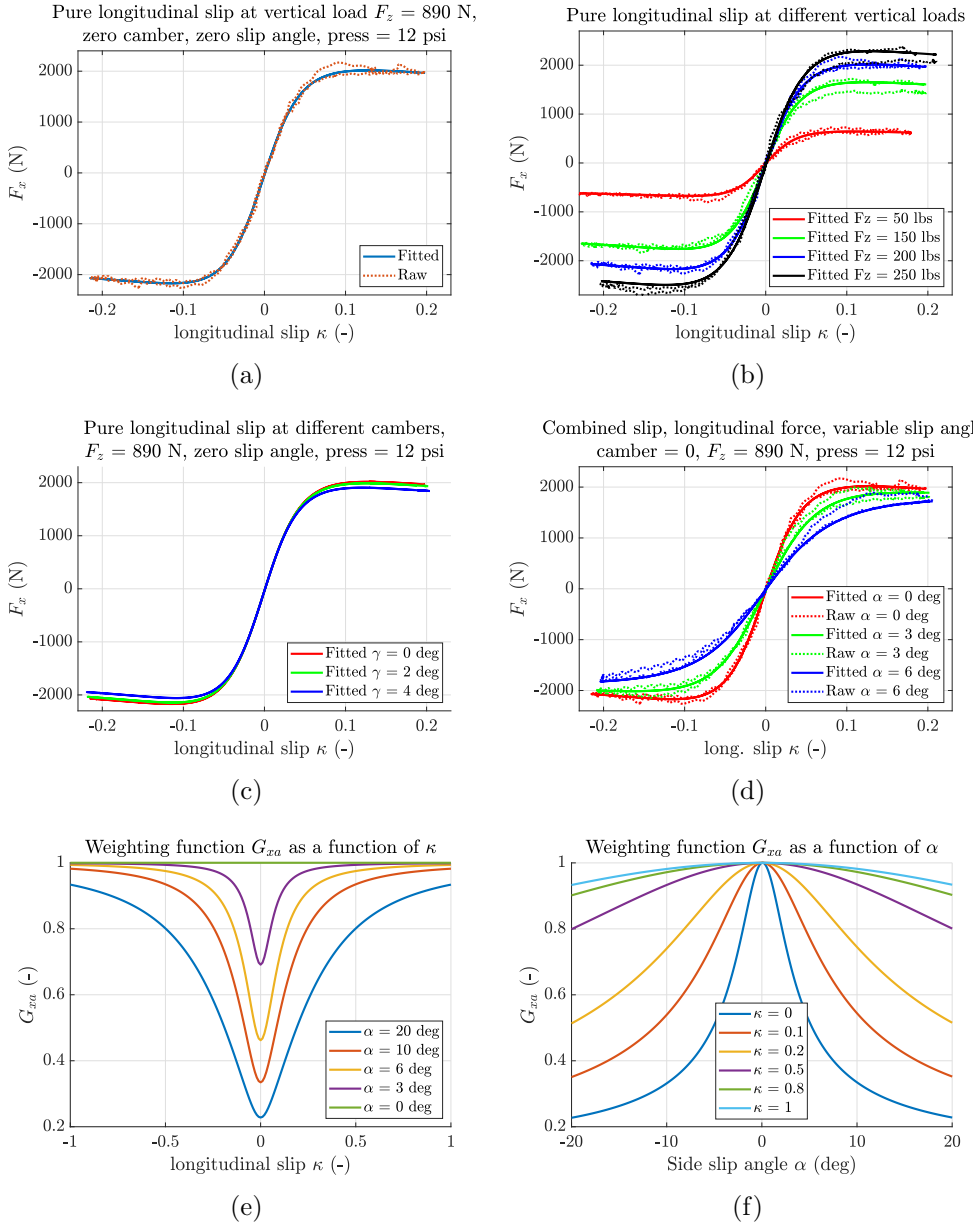

Figure 9: Fitting results, pure longitudinal slip tests (a), (b), (c), and combined tests (d), (e), (f)

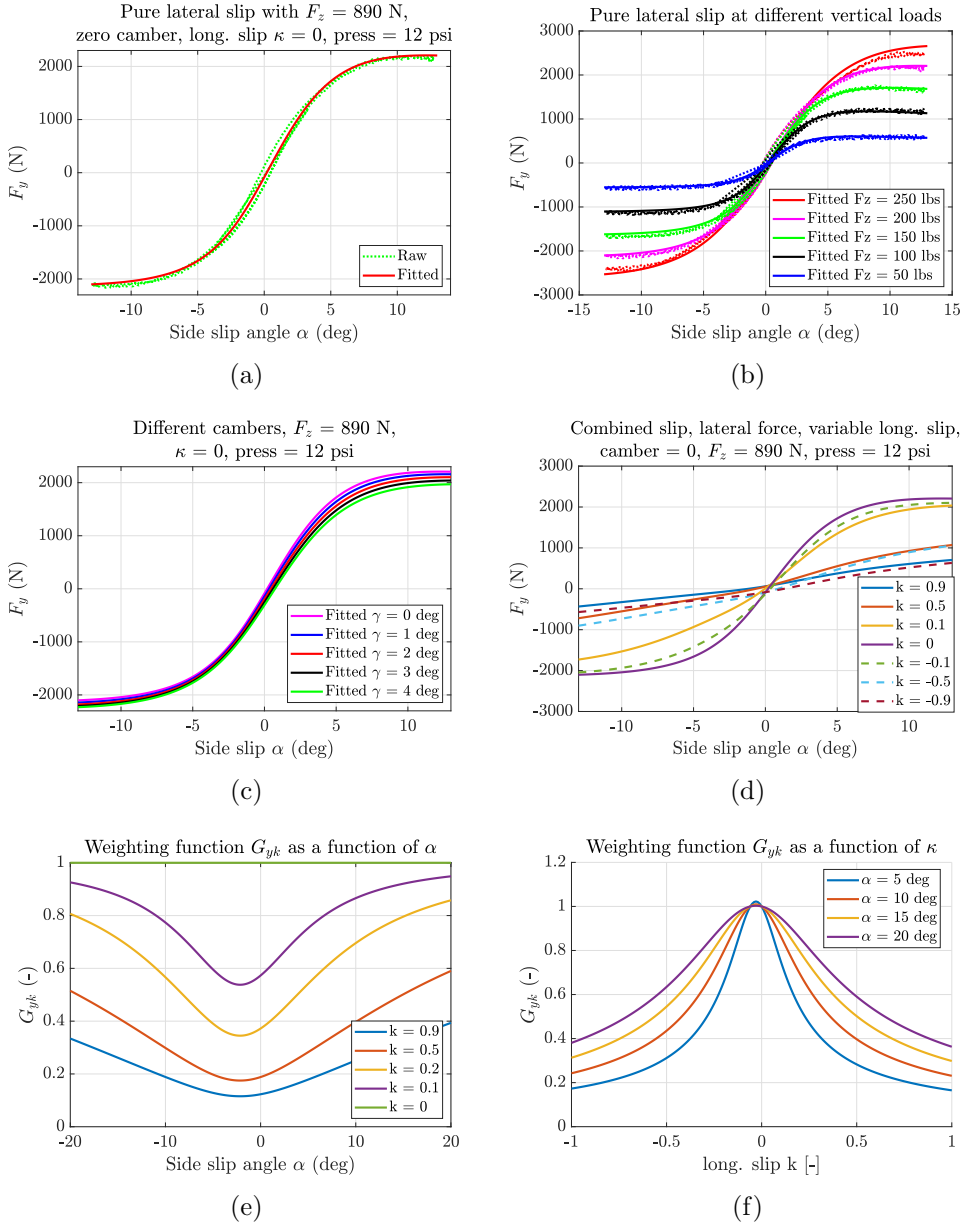

Figure 10: Fitting results for the cornering force F_y, pure lateral slip tests (a), (b), (c), and combined tests (d), (e), (f)

Referring to Figure 10 (d), notice the performance drop, in terms of cornering force F_y, when the longitudinal slip κ approaches values close to unity (which can happen during wheel lock, with $\kappa = -1$).
From Figure 10 (f) it may be seen that the peak of the weighting function G_{yk} is reached at moderate braking, and not for $\kappa = 0$. This is due to the horizontal shift S_{Hyk} in the expression of G_{yk}.

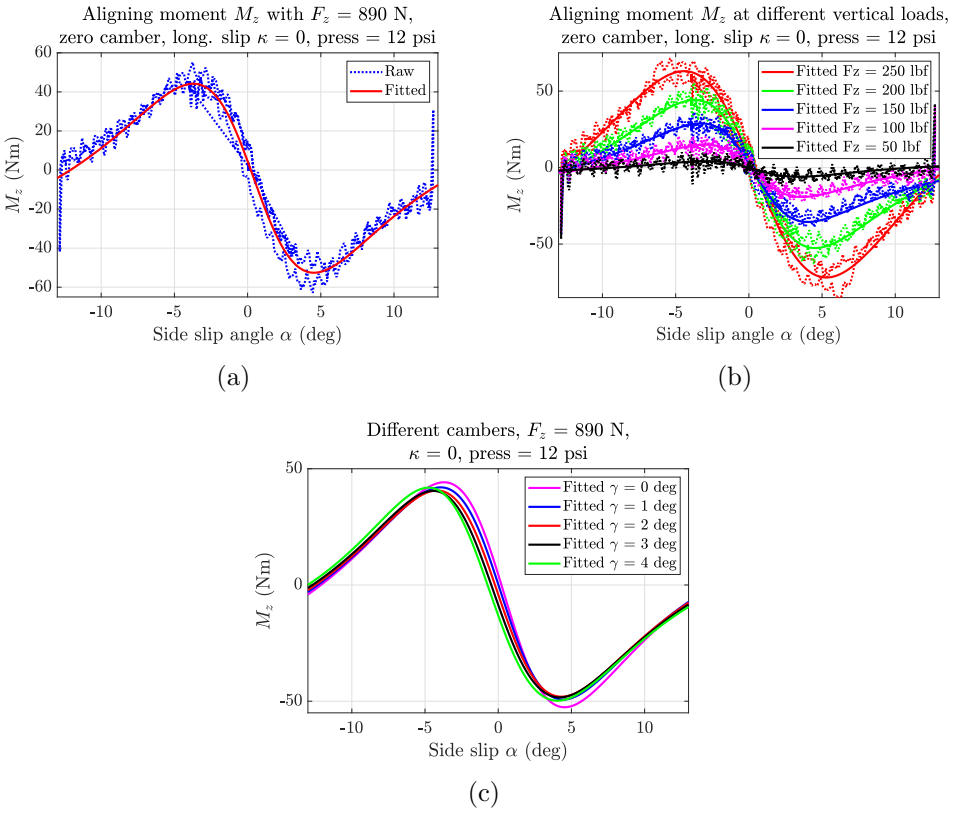

Figure 11: Fitting results, pure lateral slip tests, self-aligning torque M_z

Transient tire model

The Pacejka model previously outlined provides only a steady-state expression of the tire forces and moments.
By means of experimental measurements, it is possible to verify that the dynamics of the tire forces $\{F_x, F_y\}$ have an approximate first order evolution.
Figure 12(a) depicts the internal structure of a tire with radial design. The dynamics of the tire *carcass deformation* (see Figure 12(b)) is the main factor influencing tire transient response.

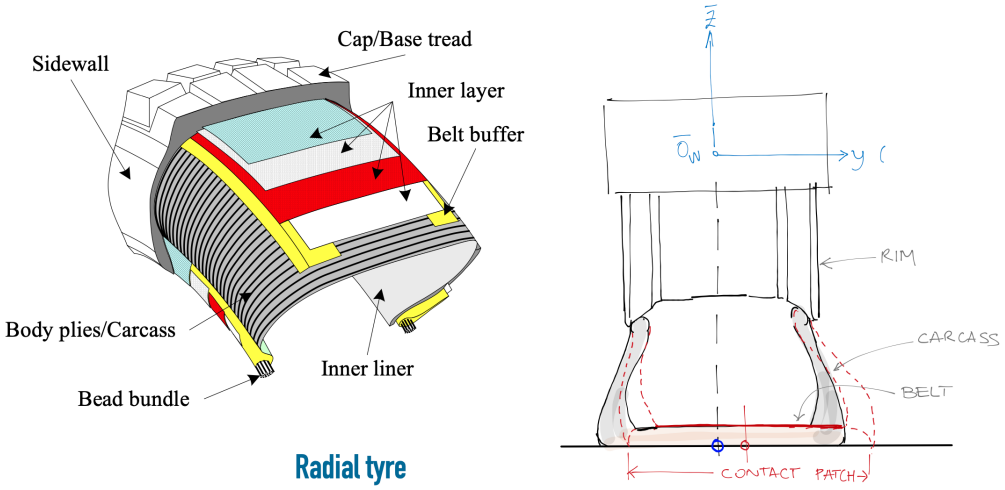

(a) (b)

Figure 12: (a) Structure of a tire with radial design, and (b) deformation of the tire carcass (sketch taken from the notes of Prof. Biral, course of Dynamics and Control of Vehicles and Robots).

The carcass deformation can be modeled as the elongation of a linear spring. Using the theory developed in Pacejka [2012], the longitudinal and lateral tire forces $\{F_x, F_y\}$ need to balance the forces due to the carcass deformation. Such force balance finally leads to two differential equations, describing the transient evolution of the longitudinal and lateral slips:

$$\begin{cases} \frac{l_x}{|u(t)|}\frac{\mathrm{d}\kappa(t)}{\mathrm{d}t} + \kappa(t) = \kappa_{ss}(t) \\ \frac{l_y}{|u(t)|}\frac{\mathrm{d}\alpha(t)}{\mathrm{d}t} + \alpha(t) = \alpha_{ss}(t) \end{cases} \tag{27}$$

In (27), l_x and l_y are the tire relaxation lengths for longitudinal and lateral dynamics, while u is the vehicle speed. Note that the quantities $\frac{l_x}{|u(t)|}$ and $\frac{l_y}{|u(t)|}$ represent the time constants of the slips dynamics. κ_{ss} and α_{ss} are the steady state values of the longitudinal and lateral slips, computed with (5) and (6). We assume that $\{l_x, l_y\}$ are constant, even if actually they depend on the tire slips and on the vertical wheel loads. It can be shown that l_x and l_y are given by:

$$\begin{cases} l_x = \frac{C_{F\kappa}}{C_{Cx}} \\ l_y = \frac{C_{F\alpha}}{C_{Cy}}, \end{cases} \tag{28}$$

with $\{C_{F\kappa}, C_{F\alpha}\}$ being the longitudinal and cornering tire stiffnesses (slopes for $\kappa = 0$ and $\alpha = 0$ of the tire force curves), while $\{C_{Cx}, C_{Cy}\}$ are the carcass stiffnesses in the longitudinal and lateral directions.

Wheel dynamics

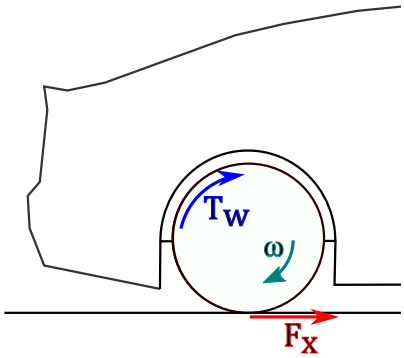

Figure 13: Forces and torques acting on a wheel body

Considering a vehicle with 4 wheels, the dynamic equations for wheels rotation about their local y axes are:

$$\begin{cases} I_{a,\mathrm{w}}\left(\frac{\mathrm{d}\omega_{rr}(t)}{\mathrm{d}t}\right) = -F_{x_{rr}}R_r + T_{w_{rr}} \\ I_{a,\mathrm{w}}\left(\frac{\mathrm{d}\omega_{rl}(t)}{\mathrm{d}t}\right) = -F_{x_{rl}}R_r + T_{w_{rl}} \\ I_{a,\mathrm{w}}\left(\frac{\mathrm{d}\omega_{fr}(t)}{\mathrm{d}t}\right) = -F_{x_{fr}}R_f + T_{w_{fr}} \\ I_{a,\mathrm{w}}\left(\frac{\mathrm{d}\omega_{fl}(t)}{\mathrm{d}t}\right) = -F_{x_{fl}}R_f + T_{w_{fl}} \end{cases} \tag{29}$$

In (29), the subscript $i \in \{f, r\}$ specifies if the corresponding wheel belongs to the front or rear axle, while $j \in \{r, l\}$ discriminates if the wheel is in the right or left side of an axle.

Longitudinal slip model for low speed

The steady-state longitudinal and lateral slip definitions (see (5) and (6)) become singular for speed values close to zero. Furthermore, the longitudinal slip differential equations (27) may induce slip (and also force) oscillations when a step input torque is applied to the wheel, at *low* speed, considering the wheel dynamic equations (29). Since the damping of the system at low speed is small, these (not physical) oscillations may last for a relatively long time.
In order to solve this issue at low speed, following Pacejka [2012] (Chapter 8.6) it is possible to introduce some artificial damping, by modifying the expression of the longitudinal slip with:

$$\kappa \longrightarrow \kappa - \frac{K_{Vlow}}{C_{F\kappa}} V_{sx} \tag{30}$$

In (30), $C_{F\kappa}$ is the longitudinal tire stiffness (slope of the F_x curve for $\kappa = 0$), while V_{sx} is the sliding velocity of the contact point with ground (2). The extra damping is added only for vehicle speed u lower than a threshold V_{low}, and K_{Vlow} gradually decreases to zero as u approaches V_{low} from the left:

$$\begin{cases} K_{Vlow} = \frac{1}{2} K_{Vlow0} \left(1 + \cos\left(\pi \frac{|u|}{V_{low}} \right) \right), & \text{if } |u| \leq V_{low} \\ K_{Vlow} = 0, & \text{if } |u| > V_{low} \end{cases} \tag{31}$$

K_{Vlow} can be seen as a damping factor that helps keeping the slip small, for speed values lower than V_{low}. With a suitable tuning of the parameter K_{Vlow0}, low speed oscillations may almost completely disappear. However, this model might give rise to some instability issues around the threshold V_{low}.
The new expression of the longitudinal slip (30) is then used to compute tire forces with Pacejka equations.

References

M. Abe. *Vehicle Handling Dynamics: Theory and Application*. Elsevier Science, 2009. ISBN 9780080961811. URL https://books.google.it/books?id=JLR8ObJp77cC.

H. Dugoff, P. Fancher, L. Segel, U. of Michigan. Highway Safety Research Institute, U. S. N. B. of Standards, and U. S. N. H. S. Bureau. *Tire Performance Characteristics Affecting Vehicle Response to Steering and Braking Control Inputs*. Michigan Highway Safety Research Institute, 1969. URL https://books.google.it/books?id=97nwPwAACAAJ.

C. Elmas, U. Guvenc, and D. Muhsin. Tire-road friction coefficient estimation and experimental setup design of electric vehicle. *Balkan Journal of Electrical and Computer Engineering*, 3, 12 2015. doi: 10.17694/bajece.88174.

M. Guiggiani. *The Science of Vehicle Dynamics: Handling, Braking, and Ride of Road and Race Cars*. SpringerLink : Bücher. Springer Netherlands, 2014. ISBN 9789401785334. URL https://books.google.it/books?id=hQrGBAAAQBAJ.

R. Jazar. *Vehicle Dynamics: Theory and Application*. Engineering (Springer-11647; ZDB-2-ENG). Springer, 2008. ISBN 9780387742434. URL https://books.google.it/books?id=Pvsv78xj7UIC.

H. Pacejka. *Tyre and Vehicle Dynamics*. Automotive engineering. Butterworth-Heinemann, 2012.

H. B. Pacejka. The tyre as a vehicle component. 1996.